Railroad Ballast Evaluation Using Ground-Penetrating Radar

Laboratory Investigation and Field Validation

Zhen Leng and Imad L. Al-Qadi

Ballast fouling in the railroad substructure is detrimental to the effectiveness of the railroad track and its structural capacity. The early detection of ballast fouling is of utmost importance to the safety of the rail system and its life-cycle cost-effectiveness. Ground-penetrating radar (GPR), a nondestructive evaluation tool, has shown its potential as a means of assessing the condition of the railroad substructure rapidly, effectively, and continuously. However, an unknown ballast dielectric constant and an unclear interface between clean and fouled ballast limit the accuracy of GPR assessment. In the present study, controlled laboratory testing was conducted to measure accurately the dielectric constants of two common ballast types, granite and limestone, under various fouling and moisture conditions. In addition, a time–frequency method, short-time Fourier transform (STFT), was used to demonstrate graphically the frequency energy variation with the depth of the ballast under various conditions. This method indirectly reflects the ballast fouling condition. To validate the effectiveness of STFT for ballast fouling assessment, field GPR data from the Orin Subdivision in Wyoming were analyzed with the STFT technique and laboratory-measured dielectric constants. Comparison of the ground truth data and GPR measurements proved that the STFT method is effective and that its results are reasonably accurate when it is used to locate fouling and trapped water within ballast, especially when the laboratory-predicted ballast dielectric constants are used in the analysis.

Railroad ballast plays an important role in supporting heavy rail loading, preventing track deformation, and providing water drainage from the track structure. However, over time, the ballast is fouled by the breakdown of ballast or the infiltration of fines, which undermines the ballast functions and which may result in damage to the rail system. The early detection of fouled ballast and measurement of the thickness of the intact ballast are vital for the safety of the rail system and could be used to optimize the life-cycle cost of the ballast system. Traditionally, a selective ground truth (drilling) method is used to measure the thickness of the ballast and evaluate its condition. However, this method is condition driven and time-consuming. In addition, it does not provide a continuous measurement. The use of ground-penetrating radar (GPR), a nondestructive method, however, has shown its potential for assessment of the condition of the track substructure rapidly, effectively, and continuously.

To improve the accuracy of assessing the railroad substructure by the use of GPR, various research studies have been conducted to optimize the GPR equipment setup and develop innovative data-processing and analysis techniques. Jack and Jackson used 450- and 900-MHz GPR antennae to provide the image attributes of the ballast and subgrade (*1*). A fixed electromagnetic (EM) velocity of 5.1×10^8 in./s (1.3×10^8 m/s) was used in the study to estimate the thickness of a ballast layer. The results showed that significant horizons can be imaged, the character changes along those horizons can be correlated with quality or structural variations, and the consistency of the depth of clean ballast could be monitored. Olhoeft and Selig (*2*) and Sussmann (*3*) used 1-GHz air-coupled antennae to map the condition of the rail track substructure. They concluded that with the proper application of GPR, substructure conditions could be observed, including the thickness of the ballast and subballast layers, variations in layer thickness along the track, and the presence of water pockets trapped in the ballast and soft subgrade because of the high water content. The frequency spectrum and frequency sum techniques were used by Clark et al. (*4*) and Silvast et al. (*5*) to assess ballast under various fouling conditions. Roberts et al. (*6*) and Al-Qadi et al. (*7*) analyzed the ballast fouling condition using scattering information of the void space in ballast aggregates and 2-GHz frequency antennae. The GPR data showed that clean ballast could potentially be distinguished from fouled ballast by the intensity of the void scattering. Al-Qadi et al. recently used various data analysis techniques to assess railroad ballast using ultrawideband GPR in a high radio-frequency environment (*8*).

It is evident that the use of GPR for the assessment of ballast condition has many obvious advantages: (*a*) it is nondestructive, which means no disturbance will be caused to the railroad structure; (*b*) it collects continuous data instead of discrete data at selective locations like the traditional drilling method does; (*c*) data collection can be conducted rapidly; for example, when the air-coupled antennae are mounted on special vehicles, the data can be collected at speeds of up to 100 mph (*9*); and (*d*) it causes very limited interruption to train traffic.

Although GPR is a great tool for the assessment of the condition of the ballast, its limitations should also be emphasized so that its benefits will not be oversold. First, the dielectric constant of the field ballast, which determines the EM wave travel speed within ballast, is unknown in most field evaluation cases. In practice, the ballast dielectric constants are usually assumed, which limits the accuracy of ballast thickness estimation and, potentially, the accurate location of fouling. Second, the gradation of the ballast usually changes grad-

Z. Leng, Department of Civil and Environmental Engineering, and I. L. Al-Qadi, Illinois Center for Transportation, University of Illinois at Urbana–Champaign, 205 North Mathews, MC-250, Urbana, IL 61801. Corresponding author: I. L. Al-Qadi, alqadi@uiuc.edu.

Transportation Research Record: Journal of the Transportation Research Board, No. 2159, Transportation Research Board of the National Academies, Washington, D.C., 2010, pp. 110–117.
DOI: 10.3141/2159-14

ually along the depth, and there is no clear interface between the fouled and the clean ballast. However, reflection of the GPR signal can happen only at the interface, where there is a significant contrast of dielectric properties. Therefore, it is not unusual for the interface between the fouled and the clean ballasts to be invisible in the GPR data. Third, the GPR data for field ballast might be affected by noises from various sources, such as reflections from rails and sleepers as well as radio interference. These noises could mask the information in GPR data useful for assessment of the condition of the ballast.

The objective of the study described here is to investigate the approaches used to overcome the first two limitations mentioned above. Controlled laboratory testing was first conducted to determine accurately the dielectric constants of two types of ballast, granite and limestone, under various fouling and moisture conditions. A time–frequency method, short-time Fourier transform (STFT), was then applied to track the change in frequency energy over the depth for ballast under various fouling and moisture conditions. This change indirectly reflects the ballast fouling condition. In the end, field GPR data collected from the Orin Subdivision in Wyoming were analyzed by use of the STFT technique and the laboratory-measured dielectric constants to validate the effectiveness of the STFT method. To address the third limitation, techniques such as optimizing the GPR equipment setup during data collection and improving the signal filtering techniques can be considered (*8*), but they are outside the scope of this paper.

GPR AND ITS APPLICATION TO ASSESSMENT OF RAILROAD BALLAST FOULING

Currently, various types of GPR systems are available on the market: frequency-modulated GPR, synthetic GPR, stepped-frequency GPR, synthetic aperture GPR, and impulse (or pulsed) GPR (*10*). However, most GPR systems used for railway applications are impulse systems, which send short time-domain EM pulses and receive the reflected pulses by an appropriate receiver. For railroad ballast, the reflected pulses could come from various sources: (*a*) the ballast surface (Signal S2 in Figure 1), in which the reflection amplitude is dependent on the dielectric constant of the clean ballast; (*b*) local scatters, that is, air voids within clean ballast (Signal S3 in Figure 1); and (*c*) the interface between clean ballast and fouled ballast or subballast if it is clear (Signal S4 in Figure 1). Signal S1 in Figure 1 represents the signal directly transmitted from the transmitter to the receiver.

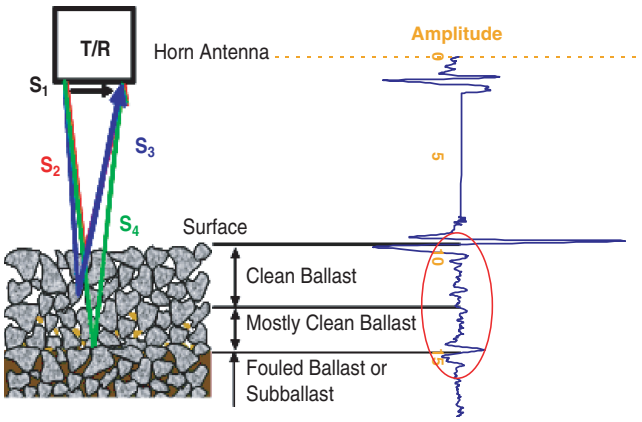

FIGURE 1 Typical GPR signal from ballast (*11*) (T = transmitter; R = receiver).

The right-hand side of Figure 1 shows an example of a single-scan GPR signal collected from ballast by using a 2-GHz air-coupled antenna. The data within the circled area could be used to extract ballast fouling information. However, it should be noted that the information contained in the circled area is dependent on not only the air void distribution (size and shape) within the ballast (i.e., the fouling condition) but also the antenna frequency. Only when the air void size is close to the wavelength of the EM pulse, which is inversely proportional to the frequency, the air void can generate significant scattering to the GPR signal. According to Xie et al., the air void size of clean ballast is comparable to the wavelength of the 2-GHz antenna; therefore, significant scattering from air voids in clean ballast can be observed in the 2-GHz data. However, the void scattering is barely observable in 1-GHz data (*11*).

To determine the thickness of clean ballast, the travel speed of the EM wave and the time within the ballast layer must be known. The travel speed of the EM wave can be determined from the dielectric constant of the ballast according to the following equation:

$$v = \frac{c}{\sqrt{\epsilon_r}} \tag{1}$$

where

v = wave propagation velocity,
c = speed of light in free space (1.2×10^{10} in./s = 3×10^8 m/s), and
ϵ_r = dielectric constant of the medium.

Therefore, to determine the thickness of the ballast, its dielectric constant must be known. However, in practice, the dielectric constants of ballast are usually unknown, which limits the accuracy of ballast thickness estimation. To improve the accuracy, controlled laboratory testing was conducted in the study to measure the dielectric constants of two commonly used ballast aggregates, limestone and granite.

Once the dielectric constant is known, the thickness of the ballast can be calculated by using the following equation:

$$d = \frac{vt}{2} = \frac{ct}{2\sqrt{\epsilon_r}} \tag{2}$$

where d is the thickness of the ballast, and t is the two-way travel time of the GPR signal within the ballast. The two-way travel time is easy to determine when the interface between clean and fouled ballast is clear. However, in most field cases, the gradation of the ballast gradually changes, and there is no clear interface between fouled and clean ballast. Correspondingly, in the time-domain GPR data, the interface between fouled and clean ballast will not be easily observed, especially when the signal is affected by possible noises. Therefore, appropriate data analysis techniques are needed for the raw GPR data to determine the ballast fouling depth accurately. STFT, a time–frequency method whose performance was investigated in this study, is a promising technique.

SHORT-TIME FOURIER TRANSFORM

STFT may keep data information in both the time and the frequency domains, and it can effectively track the frequency spectrum change with time (*12*). The information on frequency spectrum change with time is obtained by using Equation 3:

$$\mathrm{STFT}(t, \Omega) = \int_{\tau} [x(\tau) \cdot w(\tau - t)] \cdot e^{-j\Omega t} d\tau \tag{3}$$

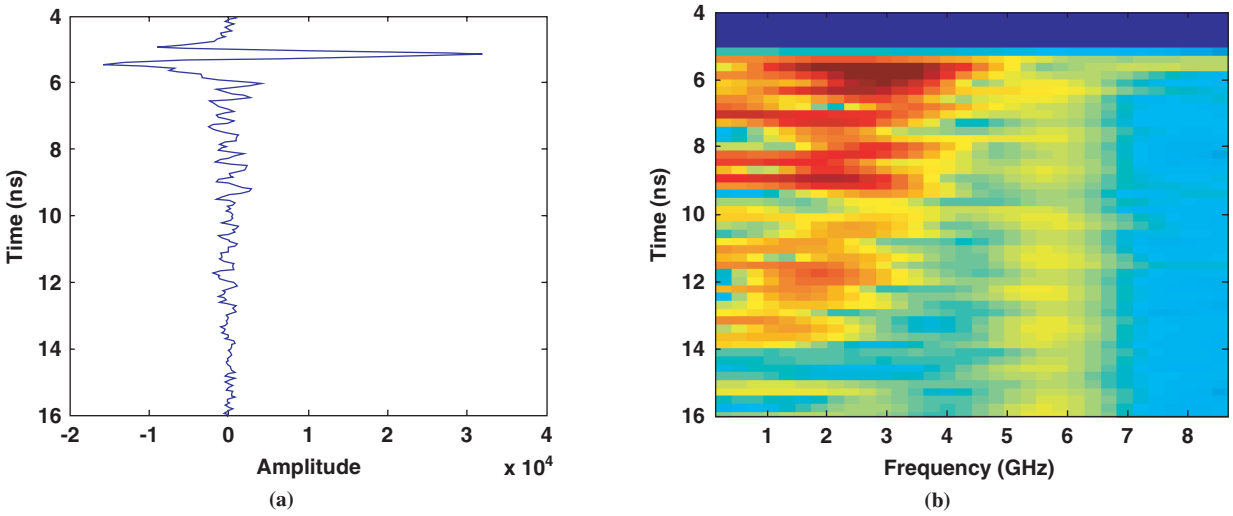

FIGURE 2 STFT spectrum example: (*a*) GPR signal in time domain and (*b*) STFT spectrum of GPR signal.

where

x = reflected signal,
t = time variable,
τ = time variable of reflected signal,
Ω = radial frequency variable,
w = window function, and
STFT = frequency energy at time t and frequency Ω.

Once STFT is calculated, it can be plotted against t and Ω. For example, Figure 2*b* is the STFT spectrum for the time-domain signal in Figure 2*a*. In Figure 2*b,* the magnitude of the frequency energy is plotted in different colors. A hot color (red or dark on a gray scale) represents high energy and a cold color (blue or light on a gray scale) represents low energy. If the dielectric constant of the medium is known, the time axis can easily be transformed to depth by using Equation 2.

LABORATORY INVESTIGATION

The first phase of this study was to build the dielectric constant profiles and STFT spectra for ballast under various fouling and moisture conditions through laboratory testing.

Testing Material and Experimental Program

As shown in Figure 3, two wooden boxes $5 \times 5 \times 4$ ft ($1.5 \times 1.5 \times 1.2$ m) were built as ballast containers for the laboratory testing. To avoid the introduction of possible noises to the GPR signal, all the screws in the boxes were made of fiberglass instead of metal material. Two common ballast types, limestone and granite, were tested, and dry clay was used as the fouling material. However, it should be noted that the fouling material in the field might be different. Hence, the conclusions of this study might not be completely applicable to cases in which the fouling material is different. GPR data collection was performed with 2-GHz air-coupled antennae and a SIR-20 GPR data acquisition unit (developed by Geophysical Survey Systems, Inc.). For each ballast type, the following testing procedure was followed:

- Place and compact 12-in.-thick (305-mm-thick) clean dry ballast in the box. Calculate the ballast air void and collect the GPR data.
- Distribute dry clay into the ballast at four levels: 10%, 25%, 40%, and 50% of the air void volume. Vibrate the ballast to permit the penetration of the clay into the bottom. Collect GPR data for each fouling level. To uniformly distribute the fouling material, the surface of the ballast was divided into small grids 1×1 ft (0.3×0.3 m), and the same amount of clay was applied to each grid (Figure 4).
- Place and compact another 12-in.-thick (305-mm-thick) clean dry ballast on top of the 12-in.-thick (305-mm-thick) 50% fouled ballast and collect GPR data.
- Place and compact 12-in.-thick (305-mm-thick) clean dry ballast on top of the 24-in.-thick (610-mm-thick) partially (25%) fouled ballast and collect GPR data.

FIGURE 3 Wooden box and 2-GHz air-coupled antennae used for ballast testing.

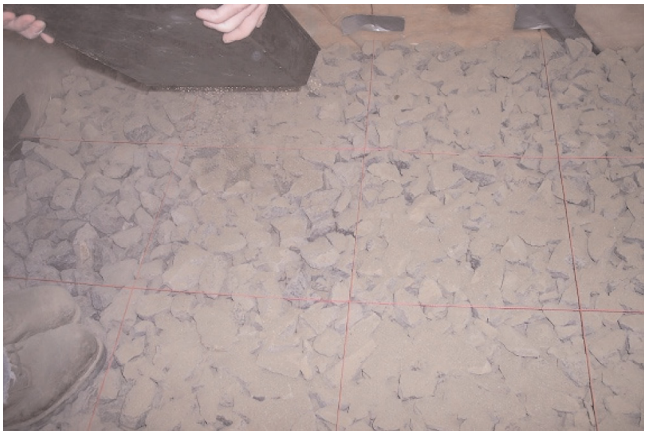

FIGURE 4 Distributing clays into ballast.

FIGURE 5 Spraying water into ballast.

- Evenly spray water into the 36-in.-thick (915-mm-thick) ballast at a level of 10%, 25%, 40%, or 50% by air void volume of the bottom 12-in.-thick (305-mm-thick) clean ballast, and collect GPR data at each moisture level. The water application was conducted by using a 5-gal (18.9-L) water sprayer (Figure 5).

As shown in Figure 6, both ballast and fouling materials were dried on the ground by an infrared heater for at least 24 h. Before the fouling material was applied, both granite and limestone ballast were uniformly graded with an aggregate size of 2.5 in. (63.5 mm). The resultant ballast air voids after compaction were 36.3% for granite and 37.8% for limestone.

Laboratory Testing Results

According to Equation 2, the dielectric constant of ballast can be calculated by using Equation 4 when the ballast thickness is known:

$$\epsilon_r = \left(\frac{ct}{2d}\right)^2 \tag{4}$$

In this study, the thickness of the tested ballast was measured by using vertical scales placed at the four corners of the wooden box.

Figure 7 presents the measured dielectric constants of two ballast materials under a dry condition and at various fouling levels. According to Figure 7, the following findings can be observed:

- Granite ballast has a smaller dielectric constant than limestone ballast at the same fouling level.
- The dielectric constant of bulk ballast increases with the increase in the fouling level.
- A strong linear relationship exists between the ballast dielectric constant and the fouling level for both ballast materials. For any fouling level between 0 and 50%, the equations shown in Figure 7 can be used to predict the dielectric constant of dry ballast.

Figure 8 shows the measured bulk dielectric constants of ballast with 13% fouling material at various moisture contents. As the moisture content increases, the bulk dielectric constant of the ballast increases significantly. There is a strong linear relationship between the dielectric constant and the moisture content. When the moisture content by volume of air void increases from 0% to 15%, the increases

(a) (b)

FIGURE 6 Material drying on ground with an infrared heater.

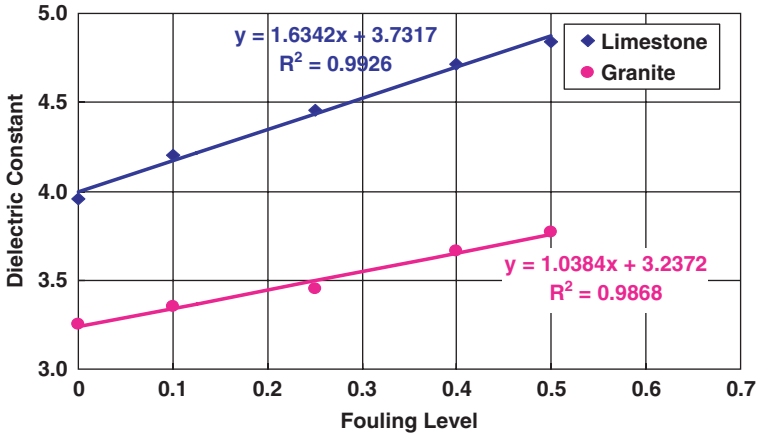

FIGURE 7 Dielectric constants of ballasts fouled by various percentages of dry clay.

in the dielectric constants are from 3.9 to 9.1 and from 4.2 to 10.5 for granite and limestone, respectively.

In addition to the dielectric constant measurement, laboratory testing data were also used to build the STFT color maps for ballasts at various fouling and moisture levels. The STFT color maps for several typical cases are presented in this paper to demonstrate how the STFT method works for ballast fouling and moisture condition assessment.

Figure 9*a* is the STFT spectrum for 36-in.-thick (915-mm-thick) dry clean ballast. It is clear that the frequency energy attenuates gradually and relatively smoothly for clean ballast. However, in Figure 9*b,* which presents the STFT spectrum for 24-in.-thick (610-mm-thick) dry clean ballast on top of 12-in.-thick (305-mm-thick) 50% fouled ballast, a sudden energy drop can be observed at about 26 in. (635 mm). This indicates that the 11-in.-thick (279-mm-thick) ballast at the bottom is fouled. The dry clay, which was applied to fill 50% of the 12-in.-thick (305-mm-thick) clean ballast air void volume, actually filled 10 in. (254 mm) instead of 100% filling of 6 in. (152 mm). This was considered reasonable, as the air voids were 60% filled. For the same ballast shown in Figure 9*b,* when 50% water by the air void volume of the 12-in.-thick (305-mm-thick) ballast was applied, the STFT spectrum in Figure 9*c* was obtained. Compared with the STFT spectrum in Figure 9*b,* a high-energy area (hot color) was observed at the bottom. The high energy is an indication of water accumulation at this location, which resulted in strong signal reflection.

FIELD VALIDATION

To further validate the effectiveness of the STFT method for ballast assessment by the use of GPR data, the field GPR data collected at the Orin Subdivision in eastern Wyoming were analyzed. As shown in Figure 10, the GPR data were collected by using 2-GHz air-coupled antennae mounted on a high-rail vehicle suspended above the rail track. The same data collection system used in the laboratory testing (GSSI SIR-20) was used. To reduce the influence of the rails and ties, the antennae were placed 2 ft (600 mm) away from the rails, which actually collected data from the shoulders of the railroad ballast. Field ballast samples were also collected at 6-in.-deep (152-mm-deep) intervals from the shoulders at selective locations. The aggregate type of the railroad ballast is granite. The moisture content of the collected samples was measured, and aggregate gradation analyses were conducted. The fouling index, F_I, was calculated for each sample to measure the ballast fouling condition. According to Selig and Waters

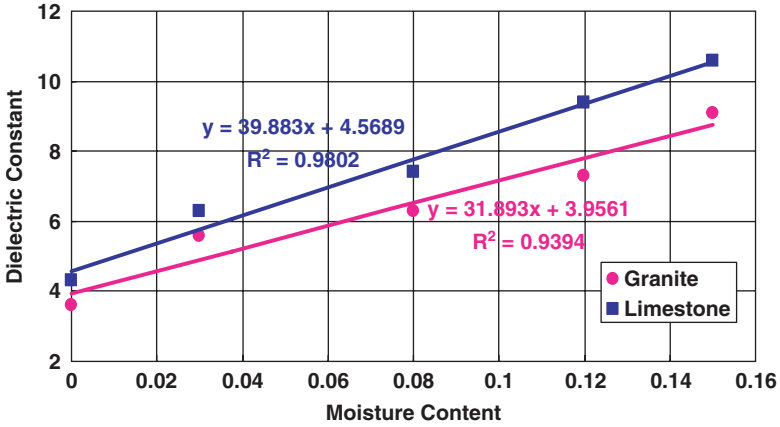

FIGURE 8 Dielectric constants of ballasts at various moisture contents.

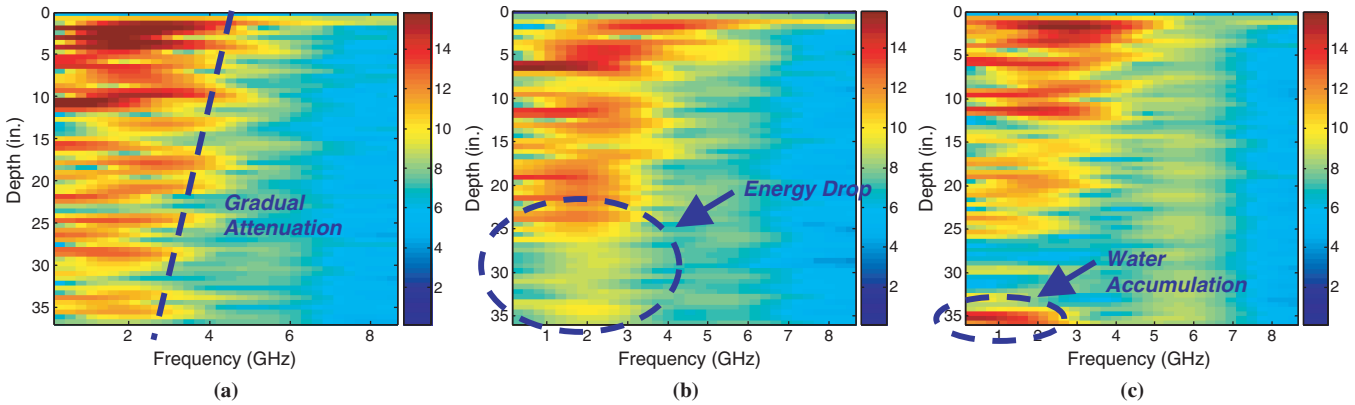

FIGURE 9 STFT spectra of ballast under various fouling and moisture conditions: (*a*) 36-in. clean ballast, (*b*) 24-in. clean ballast on top of 12-in. 50% fouled ballast, and (*c*) ballast in panel *b* with 50% water by air void volume of 12-in. clean ballast.

(*13*), the fouling index can be calculated by using the following equation:

$$F_I = P_4 + P_{200} \tag{5}$$

where P_4 represents the weight percentage of particles passing a No. 4 (4.75-mm) sieve, and P_{200} is the percentage of fine particles passing a No. 200 (0.075-mm) sieve. A value less than 10% is considered clean ballast. If the value is 10% to 20%, the ballast is moderately fouled. If the value is greater than 20%, the ballast is considered seriously fouled. Table 1 shows the fouling indexes for four cases, and Figure 11 presents their corresponding STFT color maps. The thickness of the ballast in the STFT color maps was calculated by using the laboratory-measured dielectric constants, according to their moisture content.

According to Figure 11*a,* a clear energy drop in Case 1 starts at about 25 in. (635 mm) and goes all the way down to 36 in. (915 mm), which matches well with the ground truth data in Table 1: serious ballast fouling occurs at the depth between 24 to 36 in. (610 to 915 mm). It should be noted that because the field ballast samples were collected at 6-in. (152-mm) intervals, a large fouling index could be an indication of fouling at any depth within this interval. For example, in Case 1, the fouling index for samples at the depth of 24 to 30 in. (610 to 762 mm) is 75%. It does not correspond to fouling at 24 in. (610 mm). Instead, the serious fouling could start at any depth between 24 and 30 in. (610 and 762 mm).

According to Figure 11*b,* a clear energy drop in Case 2 starts at about 15 in. (381 mm). However, a strong-energy area is located at a depth of about 20 in (508 mm), and then the energy continues dropping. In the STFT color maps, the strong-energy area corresponds to the strong reflection in the time-domain signal. Table 1 indicates that the serious ballast fouling starts at 12 to 18 in. (305 to 457 mm), which proves that the fouling location indicated by the STFT map is reasonable. The strong-energy area reflects water accumulation at 20 in. (508 mm), which is supported by the fact that there was significant rainfall before the data collection.

In Figure 11*c*, a clear energy drop occurs at 17 in. (432 mm), which is in good agreement with the ground truth data: moderate to serious fouling occurred at 12 to 18 in. (305 to 457 mm).

In Figure 11*d*, a small energy drop can be observed between 11 and 14 in. (279 and 356 mm), and a significant energy drop can be detected at about 18 in. (457 mm). The ground truth data in Table 1 indicate that the ballast material for Case 4 is moderately fouled between 12 and 18 in. (305 and 457 mm) and is seriously fouled after 18 in. (457 mm), which matches the STFT color maps very well.

As has been shown in the several case analyses described above, STFT is an effective method of providing a reasonably accurate prediction of the ballast fouling condition and water accumulation by the use of GPR data, especially when accurate dielectric constants are provided.

FIGURE 10 GPR equipment on railroad track.

TABLE 1 Fouling Indexes for Cases 1 to 4

	Percent at Depth of					
Case	0–6 in.	6–12 in.	12–18 in.	18–24 in.	24–30 in.	30–36 in.
1	1.7	1.1	2.8	7.8	75	82
2	0	0.2	106	87		
3	9.2	5.9	19.3			
4	5.6	5.0	13.8	34.8		

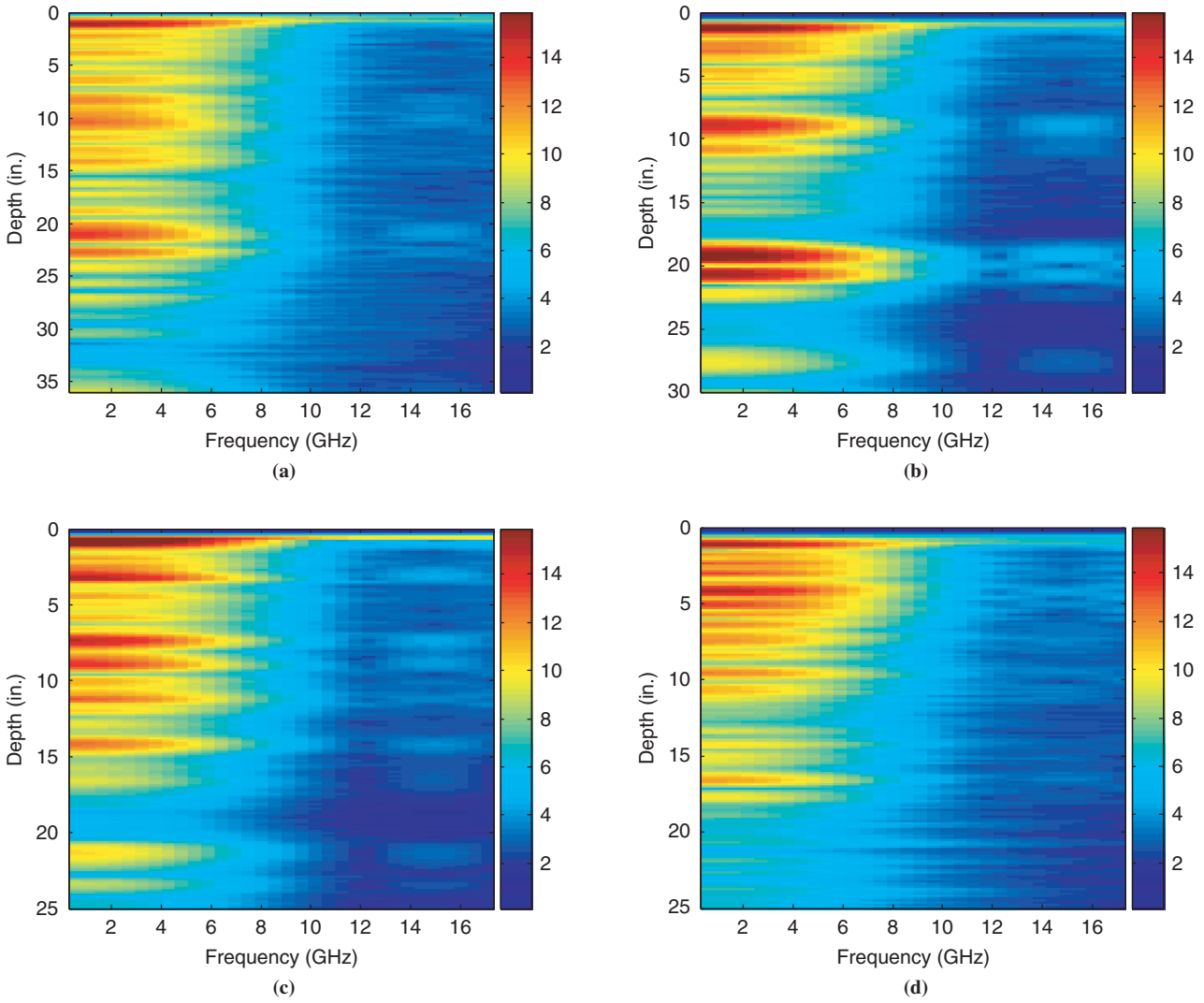

FIGURE 11 STFT color maps for (*a*) Case 1, (*b*) Case 2, (*c*) Case 3, and (*d*) Case 4.

CONCLUSIONS

In this study, controlled laboratory testing was conducted to measure the dielectric constants accurately and build STFT spectra for ballast under various fouling and moisture conditions. The laboratory-measured dielectric constants were then used for the field data analysis to validate the effectiveness of the STFT method for the assessment of ballast fouling. The following summarizes the conclusions of this study:

- Limestone ballast was found to have a greater dielectric constant than granite ballast at the same fouling level.
- At a dry clay fouling level of 0 to 50%, the dielectric constants range from 3.25 to 3.77 and 3.96 to 4.84 for granite and limestone ballast, respectively.
- The dielectric constants of ballast fouled by various percentages of dry clay can be predicted by using linear relationships, as can the dielectric constants of ballast with various moisture contents.
- Moisture can significantly increase the dielectric constant of ballast. A positive linear relationship between the bulk ballast dielectric constant and the moisture content was found.
- The STFT color map can effectively detect locations of fouling and water accumulation if an accurate dielectric constant is used, and this has been validated by both laboratory and field data.

FUTURE WORK

Although the GPR method has shown many advantages compared with the traditional drilling method for assessment of the ballast condition, it is important to recognize its limits so that the benefits of this technique will not be oversold. Detecting ballast fouling by the STFT method is based on the assumption that the GPR data collected are clean and without significant noise. However, during field data collection, many sources of noise (e.g., rails, ties, and radio signals) are generated, and this noise may mask the ballast information in the GPR data. Therefore, although GPR equipment should be properly set up during data collection, efforts are needed to further improve the GPR data filtering and data analysis techniques. To maximize the outcome of assessing ballast fouling by GPR, appropriate guidelines must be developed to assist railroad engineers with the effective use of this nondestructive testing tool.

ACKNOWLEDGMENTS

This research is sponsored by the University of Illinois at Urbana–Champaign (UIUC)–Association of American Railroad (AAR) Technology Scanning Research. The invaluable input of Roger Roberts and Erol Tutumluer is greatly appreciated. The authors also acknowledge the assistance of James Meister and the research project panel for their help and feedback during the study.

REFERENCES

1. Jack, R., and P. Jackson. Imaging Attributes of Railway Track Formation and Ballast Using Ground Probing Radar. *NDT&E International Journal,* Vol. 32, 1999, pp. 457–462.
2. Olhoeft, G. R., and E. T. Selig. Ground Penetrating Radar Evaluation of Railroad Track Substructure Conditions. *Proc., 9th International Conference on Ground Penetrating Radar,* Santa Barbara, Calif., 2002, pp. 48–53.
3. Sussmann, T. R. *Application of Ground Penetrating Radar to Railway Track Substructure Maintenance Management.* PhD thesis. University of Massachusetts, Amherst, 1999.
4. Clark, M. R., R. Gillespie, T. Kemp, D. M. McCann, and M. C. Forde. Electromagnetic Properties of Railway Ballast. *NDT&E International Journal,* Vol. 34, No. 5, 2001, pp. 305–311.
5. Silvast, M., M. Levomaki, A. Nurmikolu, and J. Noukka. NDT Techniques in Railway Structure Analysis. *Proc., World Congress on Railway Research Conference,* Montreal, Quebec, Canada, 2006.
6. Roberts, R., I. L. Al-Qadi, E. Tutumluer, J. Boyle, and T. Sussmann. Advances in Railroad Ballast Evaluation Using 2GHz Horn Antenna. *Proc., 11th International Conference on Ground Penetrating Radar* (CD), Columbus, Ohio, 2006.
7. Al-Qadi, I. L., W. Xie, and R. Roberts. Scattering Analysis of Railroad Ballast Using Ground Penetrating Radar. *Journal of Nondestructive Testing and Evaluation,* Vol. 41, No. 6, 2008, pp. 441–447.
8. Al-Qadi, I. L., W. Xie, R. Roberts, and Z. Leng. Data Analysis Techniques for GPR Used for Assessing Railroad Ballast in High Radio-Frequency Environment. *Journal of Transportation Engineering,* Vol. 136, 2010, p. 392–399.
9. Eriksen, A., J. G. Zetica, and W. Al-Nuaimy. Improved Productivity and Reliability of Ballast Inspection Using Road-Rail Multi-Channel GPR. In *Railway Engineering,* Commonwealth Institute, London, 2004.
10. Lahouar, S. *Development of Data Analysis Algorithms for Interpretation of Ground Penetrating Radar Data.* PhD thesis. Virginia Polytechnic Institute and State University, Blacksburg, 2003.
11. Xie, W., I. L. Al-Qadi, D. L. Jones, and R. L. Roberts. Development of a Time-Frequency Approach to Quantify Railroad Ballast Fouling Condition Using UWB GPR Data. Presented at 87th Annual Meeting of the Transportation Research Board, Washington, D.C., 2008.
12. Oppenheim, A. V., R. W. Schafer, and J. R. Buck. *Discrete-Time Signal-Processing.* Pearson Prentice-Hall, Englewood Cliffs, N.J., 2005.
13. Selig, E. T., and J. M. Waters. *Track Geotechnology and Substructure Management.* Thomas Telford Ltd., London, 1994.

The Railway Maintenance Committee peer-reviewed this paper.